

Hot deformation and processing maps of $\text{Al}_2\text{O}_3/\text{Al}$ composites fabricated by flake powder metallurgy

Bai-feng LUAN¹, Ri-sheng QIU¹, Chun-hong LI¹, Xiao-fang YANG¹, Zhi-qiang LI², Di ZHANG², Qing LIU¹

1. School of Materials Science and Engineering, Chongqing University, Chongqing 400044, China;
2. State Key Laboratory of Metal Matrix Composites, Shanghai Jiao Tong University, Shanghai 200240, China

Received 18 May 2014; accepted 28 January 2015

Abstract: The deformation behaviors of $\text{Al}_2\text{O}_3/\text{Al}$ composites were investigated by compressive tests conducted at temperature of 300–450 °C and strain rates of 0.001–1.0 s^{-1} with Gleeble–1500D thermal simulator system. The results show that the flow stress increases with increasing strain rate and decreasing temperature. The hyperbolic sine constitutive equation can describe the flow stress behavior of $\text{Al}_2\text{O}_3/\text{Al}$ composites, and the deformation activation energy and constitutive equations were calculated. The processing maps of $\text{Al}_2\text{O}_3/\text{Al}$ -2 μm and $\text{Al}_2\text{O}_3/\text{Al}$ -1 μm composites at strain of 0.6 were obtained and the optimum processing domains are in ranges of 300–330 °C, 0.007–0.03 s^{-1} and 335–360 °C, 0.015–0.06 s^{-1} for hot working, respectively. The instability zones of flow behavior can also be recognized by the maps.

Key words: $\text{Al}_2\text{O}_3/\text{Al}$ composites; flake powder metallurgy; flow stress; processing map

1 Introduction

Aluminum-based metal matrix composites (MMCs) have been developed as a group of advanced materials combining the good mechanical properties of Al and multifunctional properties of the ceramic reinforcements [1,2]. MMCs attract attention for structural application because of their ultra-high mechanical properties. Al_2O_3 particulates of micrometer and nanometric have been widely used in Al matrix composites. However, higher volume fraction of the ceramic particulates restricts plastic flow of the matrix alloy, leading to poorer mechanical properties as a result of the higher porosity and more severe stress concentration. The poor wettability of Al_2O_3 particulate in the metal matrix, the large surface-to-volume ratio and the uniform dispersion of Al_2O_3 particulate in Al matrix are still challenging. In order to quest for solutions that structural composites have high strength and ductility at the same time, a new technique of “flake powder metallurgy (Flake PM)” was employed to improve a uniform distribution of reinforcement [3–6]. Nevertheless, limited studies have been reported on the hot deformation behavior and

processing parameters of $\text{Al}_2\text{O}_3/\text{Al}$ composites fabricated by flake powder metallurgy [7–9]. Hence, it is necessary to evaluate the workability of the $\text{Al}_2\text{O}_3/\text{Al}$ composites.

Processing map on the basis of dynamic material model (DMM) has been widely used to understand the hot workability of many materials, especially for some materials which are difficult to deform [10]. In this mode, metal processing is considered as a system in which the workpiece material is considered as a dissipater of power. At any moment, the total power dissipation consists of two complementary parts. The G content represents the major power input dissipated in the form of the temperature increase and J co-content represents the dissipation through metallurgical process. The total power dissipated P can be calculated as

$$P = \sigma \dot{\epsilon} = G + J = \int_0^{\dot{\epsilon}} \sigma d\dot{\epsilon} + \int_0^{\sigma} \dot{\epsilon} d\sigma \quad (1)$$

where σ is the instantaneous flow stress, and $\dot{\epsilon}$ is the applied strain rate. Using this approach, it is possible not only to optimize hot workability but also to delineate regimes of flow instability which should be avoided strictly in processing.

Foundation item: Project (2012AA030311) supported by the National High-tech Research and Development Program of China; Project (2010BB4074) supported by the Natural Science Foundation of Chongqing Municipality, China; Project (2010ZD-02) supported by the State Key Laboratory for Advanced Metals and Materials, China

Corresponding author: Bai-feng LUAN; Tel: +86-23-65106067; E-mail: bfluan@cqu.edu.cn

DOI: 10.1016/S1003-6326(15)63698-6

2 Experimental

The samples of the $\text{Al}_2\text{O}_3/\text{Al}$ composites measured in this work were provided by the Shanghai Jiao Tong University, China. The atomized pure Al powder (99.5%, mass fraction) with mean particle size of about $10\ \mu\text{m}$ was selected as raw materials in the present work. As illustrated in Ref. [3], the typical fabrication of $\text{Al}_2\text{O}_3/\text{Al}$ composites by flake PM involves preparation of flake powders, the in situ introduction of Al_2O_3 and alignment and consolidation of the flake powder. Then, flake Al powders of about 2 and $1\ \mu\text{m}$ in thickness were obtained, which will be denoted as $\text{Al}_2\text{O}_3/\text{Al}-2\ \mu\text{m}$ and $\text{Al}_2\text{O}_3/\text{Al}-1\ \mu\text{m}$ specimens. A Zeiss Auriga focused ion beam scanning electron microscopy (Zeiss Auriga FIB/SEM) was used for microstructure characterization. In these cases, the specimens were electrolytically polished with a solution of 10% perchloric acid and 90% alcohol (volume fraction). The voltage of 20 V and a temperature of $25\ ^\circ\text{C}$ were adopted for polishing. The initial microstructures of the $\text{Al}_2\text{O}_3/\text{Al}-2\ \mu\text{m}$ and $\text{Al}_2\text{O}_3/\text{Al}-1\ \mu\text{m}$ specimens fabricated by flake PM are shown in Fig. 1. From the SEM images, the extruded multilayer structures with alternating Al (2 and $1\ \mu\text{m}$) and Al_2O_3 layers can be observed from the vertical section of the extrusion specimens.

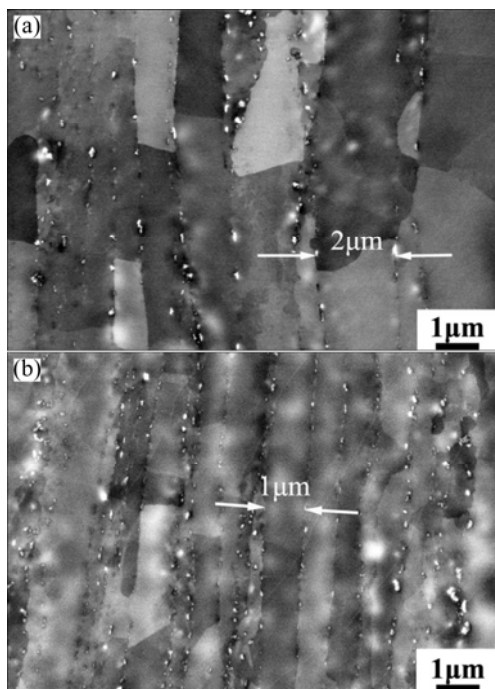


Fig. 1 Initial microstructures of $\text{Al}_2\text{O}_3/\text{Al}-2\ \mu\text{m}$ (a) and $\text{Al}_2\text{O}_3/\text{Al}-1\ \mu\text{m}$ (b) composites

Cylinder specimens with the dimensions of $d8\ \text{mm} \times 10\ \text{mm}$ were cut from the $\text{Al}_2\text{O}_3/\text{Al}-2\ \mu\text{m}$ and $\text{Al}_2\text{O}_3/\text{Al}-1\ \mu\text{m}$ specimens fabricated by Flake PM. The

hot compression tests were performed on a mechanical testing system (Gleeble–1500D) at a vacuum of 1×10^{-3} Pa. Test temperatures were selected at 300, 350, 400 and $450\ ^\circ\text{C}$ with strain rates of 0.001, 0.01, 0.1 and $1.0\ \text{s}^{-1}$, respectively. Once the compressions were completed, these specimens were immediately quenched into water and vertical section was examined for microstructure. True stress–strain curves collected automatically by the Gleeble–1500D were used to analyze the hot flow behavior and calculate hot processing maps of the experimental alloys.

3 Results and discussion

3.1 Flow stress behavior

Figures 2 and 3 present the true stress–true strain curves of the $\text{Al}_2\text{O}_3/\text{Al}-2\ \mu\text{m}$ and $\text{Al}_2\text{O}_3/\text{Al}-1\ \mu\text{m}$ composites at different strain rates and temperatures, respectively. The characteristic of the true stress–true strain curves is similar for both $\text{Al}_2\text{O}_3/\text{Al}-2\ \mu\text{m}$ and $\text{Al}_2\text{O}_3/\text{Al}-1\ \mu\text{m}$ composites. However, it can be seen that the peak stresses of flake PM $\text{Al}_2\text{O}_3/\text{Al}-1\ \mu\text{m}$ composite are higher than those of flake PM $\text{Al}_2\text{O}_3/\text{Al}-2\ \mu\text{m}$ composite. The thickness of lamellar structure of flake PM $\text{Al}_2\text{O}_3/\text{Al}-1\ \mu\text{m}$ composite is smaller than that of flake PM $\text{Al}_2\text{O}_3/\text{Al}-2\ \mu\text{m}$ composite, and the finer grains can be gained by the flake PM $\text{Al}_2\text{O}_3/\text{Al}-1\ \mu\text{m}$ composite. The matrix around the Al_2O_3 particles presents much higher dislocation density than normal alloy. More Al_2O_3 particles and smaller lamellar structures may act to hinder the recovery and recrystallization processes of Al matrix, and keep dislocations in the small grains, thus increasing the strain hardening capacity.

As shown in Fig. 2, it can be seen that the flow stresses of the $\text{Al}_2\text{O}_3/\text{Al}-2\ \mu\text{m}$ composite increase sharply with increasing strain until peak flow stress, which should be ascribed to the increase of dislocation density. These accumulated dislocations could significantly impede further deformation and thus lead to the higher strength. After the peak flow stress, stress–strain curves markedly decrease at different strain rates and high deformation temperatures (350, 400 and $450\ ^\circ\text{C}$). The flow stresses decrease later because dynamic recrystallization or recovery happens due to the formation of numerous dislocation cells or tangled structures. The characteristic of these flow stress curves can be demonstrated in terms of discontinuous yielding and flow softening phenomenon. Essentially, it is a dynamic competitive procedure between the working hardening caused by dislocation reduplication, pileup and tanglement and the softening caused by the dislocation rearrangement and the counteraction of unlike dislocation. Subsequently, the flow stresses of the alloy rise with decreasing deformation temperature at

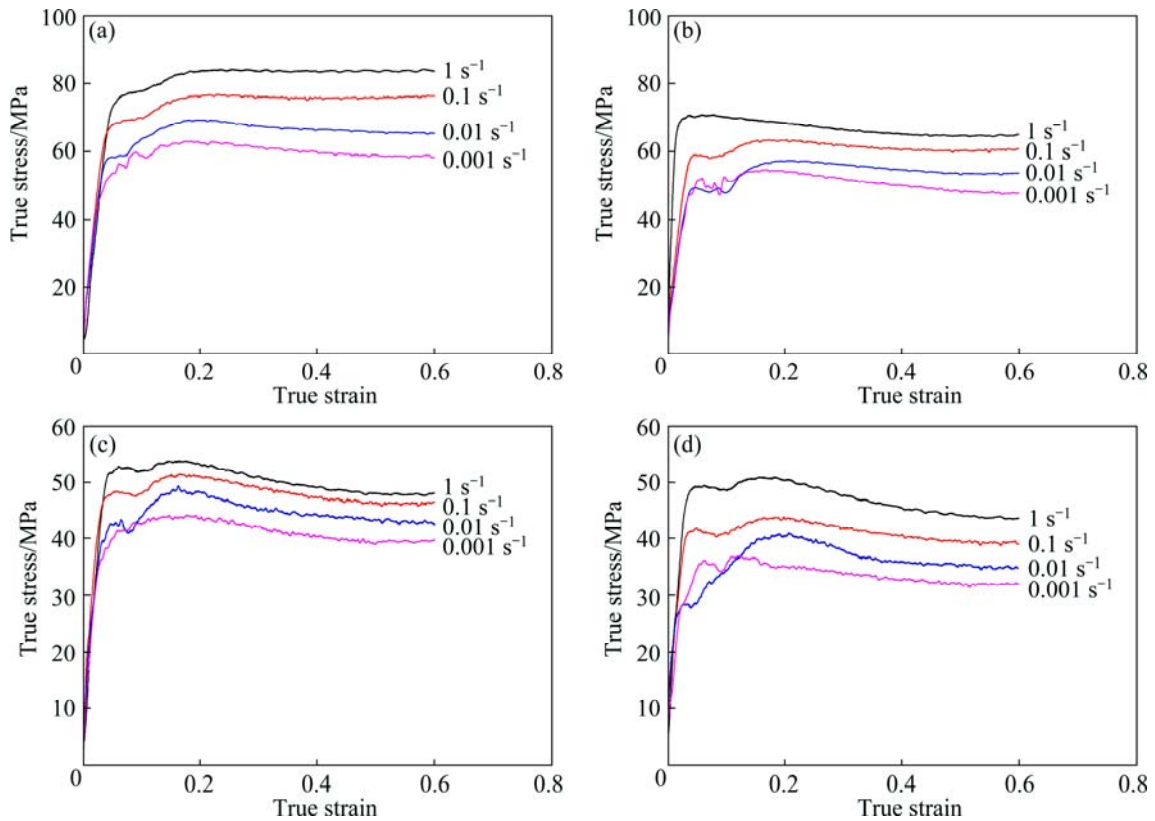


Fig. 2 True stress–true strain curves at various strain rates for $\text{Al}_2\text{O}_3/\text{Al}$ -2 μm composite: (a) 300 °C; (b) 350 °C; (c) 400 °C; (d) 450 °C

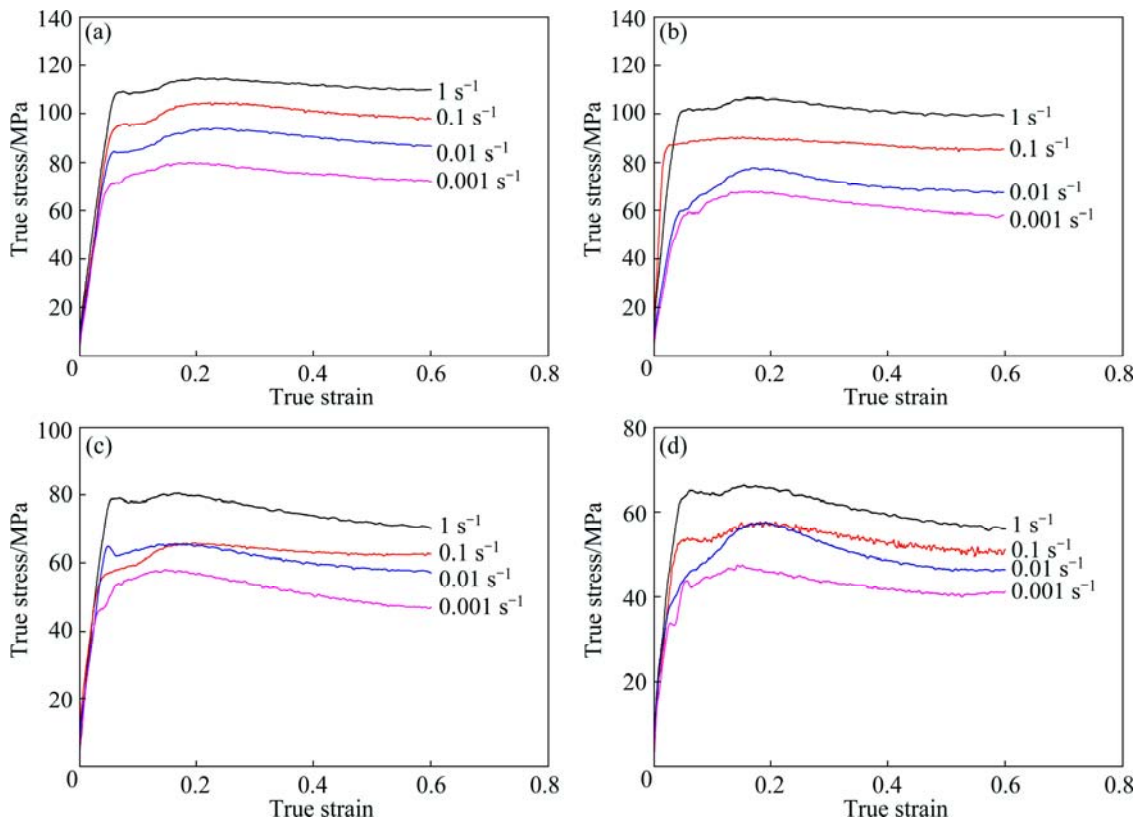


Fig. 3 True stress–true strain curves at various strain rates for $\text{Al}_2\text{O}_3/\text{Al}$ -1 μm composite: (a) 300 °C; (b) 350 °C; (c) 400 °C; (d) 450 °C

any fixed strain rate. It is suggested that higher temperature would make dislocation movement and dynamic recrystallization easier. Meanwhile, the impedance of Al₂O₃ particles to deformation will also be lowered which contributes to the lower flow stresses.

3.2 Kinetic analysis during hot deformation

To investigate the hot deformation behavior of metal materials, it is well known that constitutive equations are able to reveal the relationship of flow stress on deformation temperature and strain rate. At all the stress levels, the relationship of flow stress on deformation temperature and strain rate can be described by hyperbolic sine model proposed by SELLARS and MCTEGART [11] and ZHOU et al [12]:

$$\dot{\epsilon} = A[\sinh(\alpha\sigma)]^n \exp\left(-\frac{Q}{RT}\right) \tag{2}$$

$$Z = \dot{\epsilon} \exp\left(\frac{Q}{RT}\right) = A[\sinh(\alpha\sigma)]^n \tag{3}$$

where $\dot{\epsilon}$ is the strain rate, A and α are constants, σ is the steady flow stress, n is the stress exponent, Q is the activation energy for hot working, R is the gas constant, T is the deformation temperature and Z is the Zener-Hollomon parameter.

In order to find the material constants A , α , n and Q at strain of 0.5, various plots of flake PM Al₂O₃/Al-2 μm and Al₂O₃/Al-1 μm composites were drawn as shown in Figs. 4 and 5, respectively. It exists a linear relation to peak stress to strain rate and deformation temperature which could satisfy Eq. (2). The stress exponent n is calculated from the inverse of the slope of the $\ln \sigma$ and $\ln \dot{\epsilon}$ plot (Figs. 4(a) and 5(a)). Figures 4(b) and 5(b) are the Arrhenius plot obtained between $\ln \sigma$ and $1/T$ at various strain rates. Therefore, the estimated Q values of Al₂O₃/Al-2 μm and Al₂O₃/Al-1 μm composites are obtained to be approximate 359.9 and 252.9 kJ/mol, respectively. The activation energy for self-diffusion is 144 kJ/mol in pure Al [13,14]. In the present investigation, the activation energy is much higher than the normal value 149.7 kJ/mol for 5% Al₂O₃/Al composite [15], which may suggest that the deformation mechanism of flake PM Al₂O₃/Al composites is dominated by dynamic recrystallization instead of diffusion. The higher values of Q in the composites are due to the effect of Al₂O₃ particles which pins the motion of the dislocations and grain boundaries. The flow stress for Al₂O₃/Al-2 μm (Eq. (4)) and Al₂O₃/Al-1 μm (Eq. (5)) composites can be estimated from the constitutive equations represented by

$$\dot{\epsilon} = 2.018 \times 10^{31} [\sinh(0.0124\sigma)]^{20.83} \exp\left(\frac{-359.9}{RT}\right) \tag{4}$$

$$\dot{\epsilon} = 2.426 \times 10^{23} [\sinh(0.0093\sigma)]^{18.61} \exp\left(\frac{-252.9}{RT}\right) \tag{5}$$

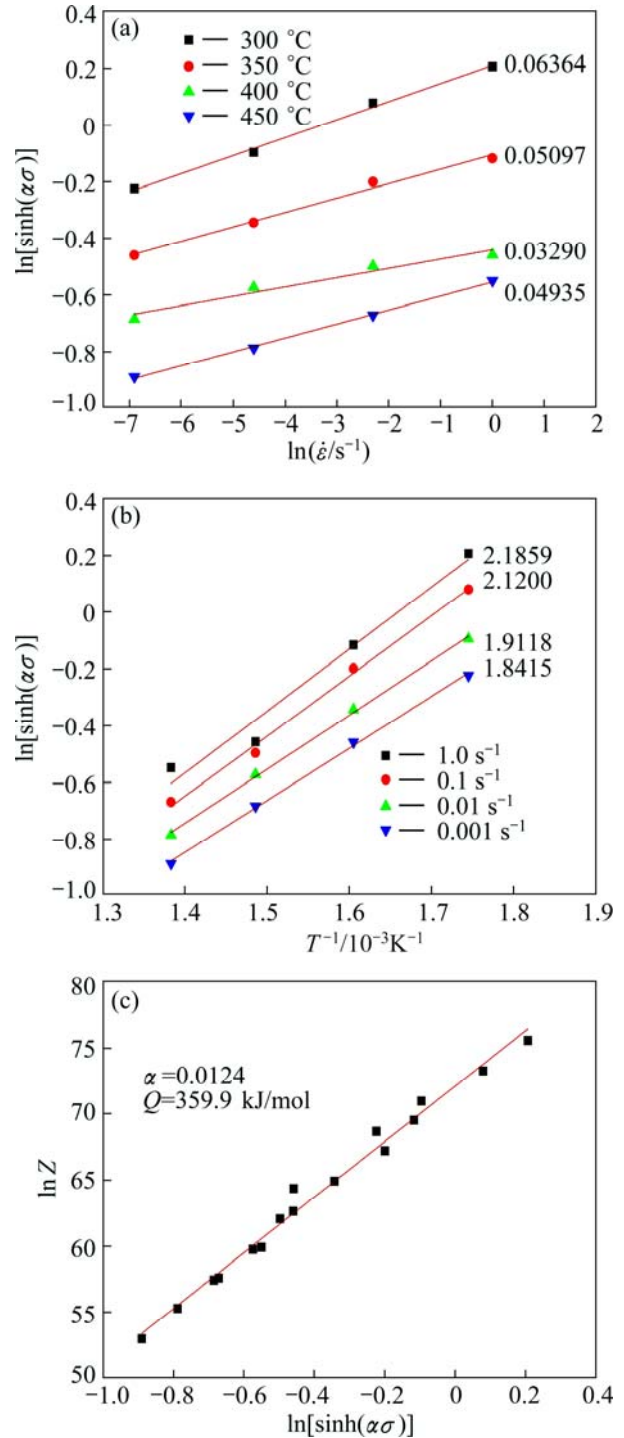


Fig. 4 Relationships between strain rate and flow stress for Al₂O₃/Al-2 μm composite: (a) $\ln[\sinh(\alpha\sigma)]$ and $\ln \dot{\epsilon}$; (b) $\ln[\sinh(\alpha\sigma)]$ and temperature; (c) $\ln Z$ and $\ln[\sinh(\alpha\sigma)]$

The variations of flow stress with Zener-Hollomon parameter for the flake PM Al₂O₃/Al-2 μm and Al₂O₃/Al-1 μm composites are plotted in Figs. 4(c) and 5(c), respectively. It can be seen from Figs. 4(c) and 5(c) that the correlation coefficients r are 0.992 and 0.989, respectively, and the rate equations are valid.

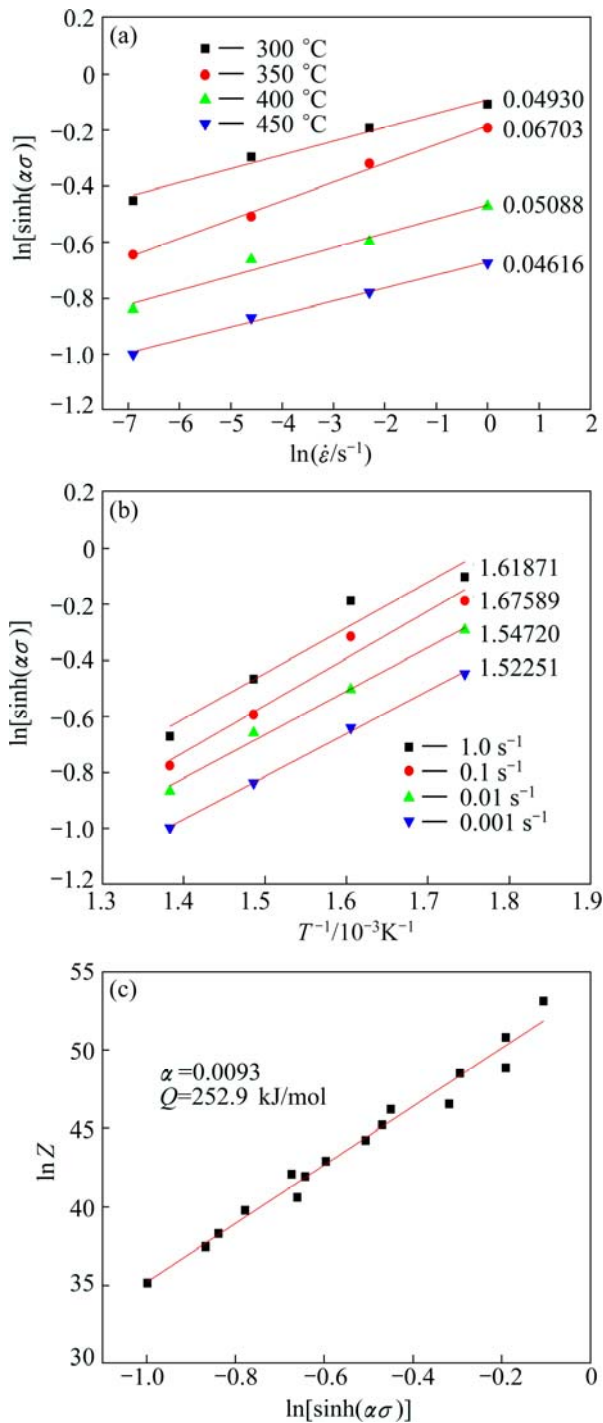


Fig. 5 Relationships between strain rate and flow stress for $\text{Al}_2\text{O}_3/\text{Al}$ -1 μm composite: (a) $\ln[\sinh(\alpha\sigma)]$ and $\ln \dot{\epsilon}$; (b) $\ln[\sinh(\alpha\sigma)]$ and temperature; (c) $\ln Z$ and $\ln[\sinh(\alpha\sigma)]$

3.3 Processing maps

The variation of a dimensionless parameter (η) called the efficiency of power dissipation can be defined as

$$\eta = \frac{2m}{m+1} \quad (6)$$

where m is strain rate sensitivity parameter of flow stress, and it is calculated as a function of $\dot{\epsilon}$. The $\ln \sigma$ versus

$\ln \dot{\epsilon}$ curve is fitted by a cubic spline.

$$m = \partial(\ln \sigma) / \partial(\ln \dot{\epsilon}) \quad (7)$$

The variation of η with temperature and strain rate constitutes a processing map, which exhibits various domains that may be correlated with specific microstructural mechanisms. The contour plot of the iso-efficiency η values on the temperature–strain rate field constitutes the processing maps, which are known as power dissipation maps. In addition to the η contours, the instability criterion is given by [10,16–18]:

$$\xi(\dot{\epsilon}) = \frac{\partial \ln[m/(m+1)]}{\partial \ln \dot{\epsilon}} + m < 0 \quad (8)$$

which is applied to delineating the temperature–strain rate regimes of flow instability on the processing map.

Processing maps of $\text{Al}_2\text{O}_3/\text{Al}$ -2 μm and $\text{Al}_2\text{O}_3/\text{Al}$ -1 μm composites at strains of 0.3, 0.4, 0.5 and 0.6 are shown in Figs. 6 and 7, respectively. The maps obtained at strains of 0.3, 0.4 and 0.5 are essentially similar to that obtained at a strain of 0.6. It indicates that strain does not have significant influence. The processing map of $\text{Al}_2\text{O}_3/\text{Al}$ -2 μm composite exhibits a clear domain occurring in the temperature range of 300–330 °C and strain rate range of 0.007–0.03 s^{-1} with peak efficiency of 12%. The map of $\text{Al}_2\text{O}_3/\text{Al}$ -1 μm composite shows a single domain in the temperature range of 335–360 °C and strain rate range of 0.015–0.06 s^{-1} , with a peak efficiency of about 18% occurring at about 350 °C and 0.03 s^{-1} . The microstructural observations confirm that dynamic recrystallization occurs under the deformation condition of those domains. For example, microstructure of $\text{Al}_2\text{O}_3/\text{Al}$ -2 μm composite specimen deformed at 300 °C and 0.01 s^{-1} is shown in Fig. 8. It shows recrystallized grains, suggesting the occurrence of dynamic recrystallization. The result is in good agreement with the prediction of the hot processing maps in Fig. 6. The microstructure of $\text{Al}_2\text{O}_3/\text{Al}$ -2 μm composite specimen revealed equiaxed grain formation, refinement of grain, and grain boundaries of irregular in nature describing the occurrence of dynamic recrystallization.

4 Conclusions

1) In the strain rate range from 0.001 to 1.0 s^{-1} and the temperature range from 300 to 450 °C, the flow stresses of $\text{Al}_2\text{O}_3/\text{Al}$ -2 μm and $\text{Al}_2\text{O}_3/\text{Al}$ -1 μm composites decrease with the increase of deformation temperature, meanwhile, increase with the increase of strain rate.

2) The hyperbolic sine constitutive equation can describe the flow stress behavior of $\text{Al}_2\text{O}_3/\text{Al}$ -2 μm and

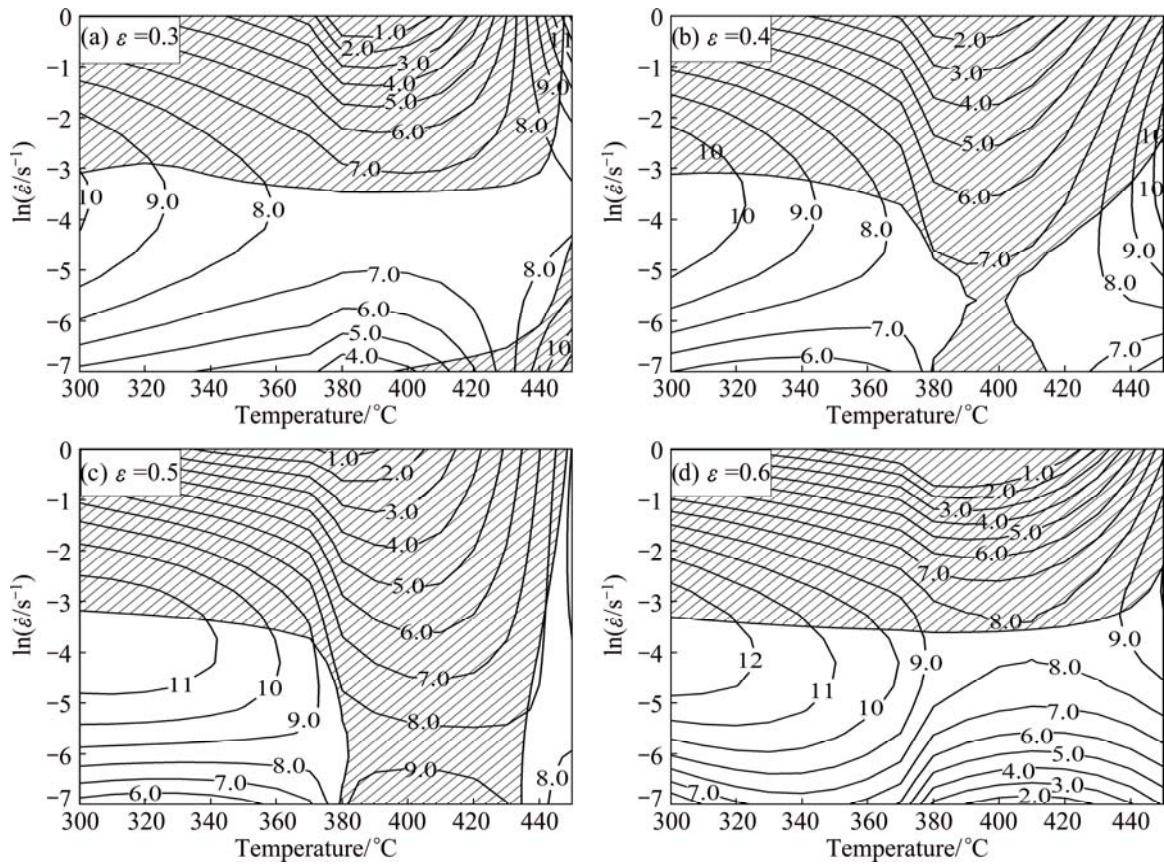


Fig. 6 Processing maps of Al₂O₃/Al-2 μm composite at different strains

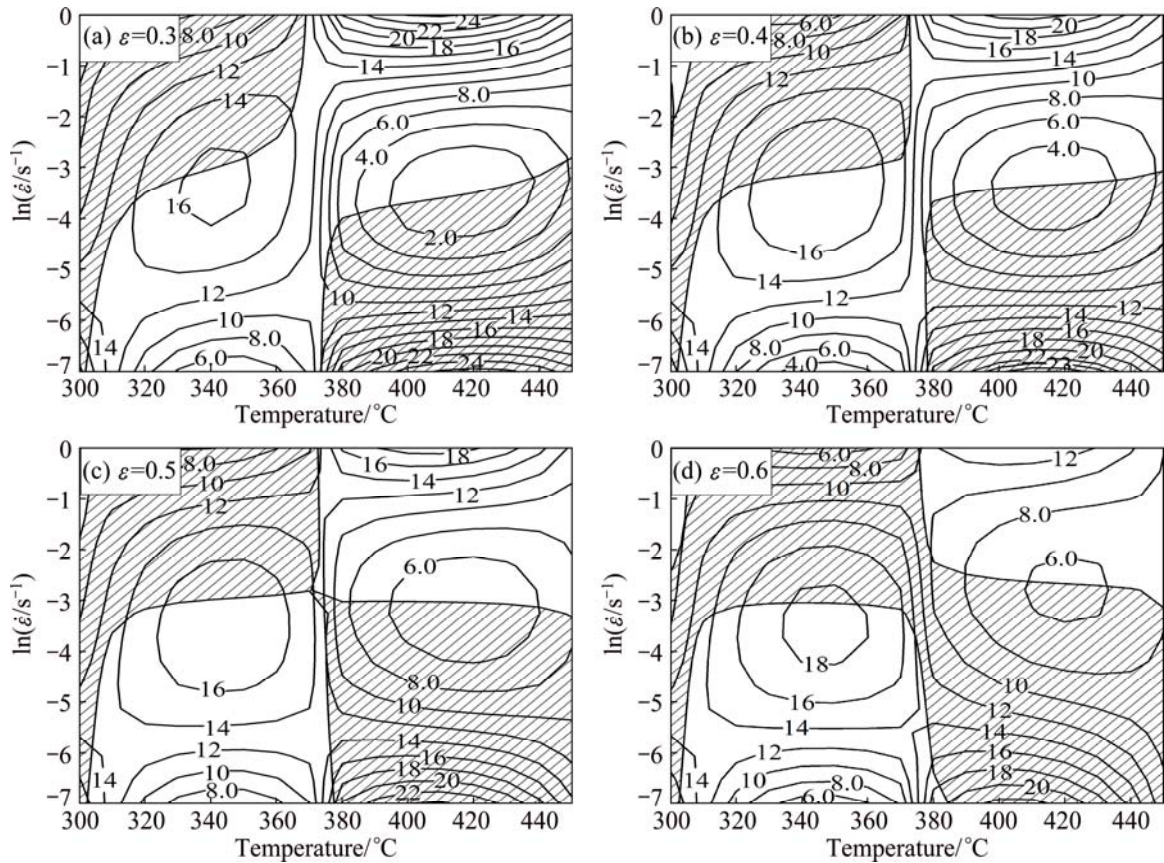


Fig. 7 Processing maps of Al₂O₃/Al-1 μm composite at different strains

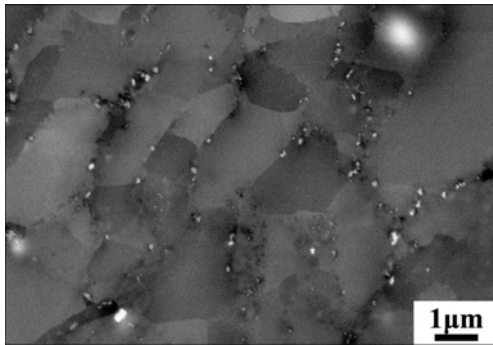


Fig. 8 Microstructure of Al₂O₃/Al-2 μm composite at 300 °C and 0.01 s⁻¹

Al₂O₃/Al-1 μm composites, the constitutive equations of Al₂O₃/Al-2 μm and Al₂O₃/Al-1 μm composites for deformation are

$$\dot{\varepsilon} = 2.018 \times 10^{31} [\sinh(0.0124\sigma)]^{20.83} \exp\left(\frac{-359.9}{RT}\right)$$

and

$$\dot{\varepsilon} = 2.426 \times 10^{23} [\sinh(0.0093\sigma)]^{18.61} \exp\left(\frac{-252.9}{RT}\right),$$

respectively.

3) The processing maps of Al₂O₃/Al-2 μm and Al₂O₃/Al-1 μm composites at strain of 0.6 exhibit safe processing domains which are in ranges of 300–330 °C, 0.007–0.03 s⁻¹ and 335–360 °C, 0.015–0.06 s⁻¹ for hot working, respectively.

Acknowledgments

The authors would like to acknowledge Mr. Fang-fang HE for valuable discussion and critical comments.

References

- [1] MIRACLE D B. Metal matrix composites-from science to technological significance [J]. *Composites Science and Technology*, 2005, 65: 436–440.
- [2] CHEN X G, DA SILVA M, GOUGEN P, ST-GEORGES L. Microstructure and mechanical properties of friction stir welded AA6063-B₄C metal matrix composites [J]. *Materials Science and Engineering A*, 2009, 518: 174–184.
- [3] LIN Jian, LI Zhi-qiang, FAN Gen-lian, ZHANG Di. A flake powder metallurgy approach to Al₂O₃/Al biomimetic nanolaminated composites with enhanced ductility [J]. *Scripta Materialia*, 2011, 65: 412–415.
- [4] KAI X Z, LI Z Q, FAN G L, GUO Q, XIONG D B, ZHANG W L, SU Y S, LU W J, MOON W J, ZHANG D. Enhanced strength and ductility in particulate-reinforced aluminum matrix composites fabricated by flake powder metallurgy [J]. *Materials Science and Engineering A*, 2013, 587: 46–53.
- [5] LIN Jian, LI Zhi-qiang, FAN Gen-lian, CAO Lin-lin, ZHANG Di. Strong and ductile carbon nanotube/aluminum bulk nanolaminated composites with two-dimensional alignment of carbon nanotubes [J]. *Scripta Materialia*, 2012, 66: 331–334.
- [6] KAI Xi-zhou, LI Zhi-qiang, FAN Gen-lian, GUO Qiang, TAN Zhan-qiu, ZHANG Wen-long, SU Yi-shi, LU Wei-jie, MOON W J, ZHANG Di. Strong and ductile particulate reinforced ultrafine-grained metallic composites fabricated by flake powder metallurgy [J]. *Scripta Materialia*, 2013, 68: 555–558.
- [7] WANG Yuan-zhu. Comment on “characteristics of superplasticity domain in the processing map for hot working of an Al alloy 2014–20vol.% Al₂O₃ metal matrix composite” [J]. *Materials Science and Engineering A*, 1996, 212: 178–181.
- [8] PARK B G, CROSKY A G, HELLIER A K. Material characterisation and mechanical properties of Al₂O₃-Al metal matrix composites [J]. *Journal of Materials Science*, 2001, 36: 2417–2426.
- [9] AGHAJANIAN M K, LANGENSIEPEN R A, ROCAZELLA M A, LEIGHTON J T, ANDERSSON C A. The effect of particulate loading on the mechanical behaviour of Al₂O₃/Al metal matrix composites [J]. *Journal of Materials Science*, 1993, 28: 6683–6690.
- [10] PRASAD Y V R K, GELEL H L, DORAIVELU S M, MALAS J C, MORGAN J T, LARK L A, BARKER D R. Modeling of dynamic materials behavior in hot deformation: forging of Ti 6242 [J]. *Metallurgical Transactions A*, 1984, 15: 1883–1892.
- [11] SELLARS C M, MCTEGART W J. On mechanism of hot deformation [J]. *Acta Metallurgica*, 1966, 14: 1136–1138.
- [12] ZHOU H T, LI Q B, ZHAO Z K, LIU Z C, WEN S F, WANG Q D. Hot workability characteristics of magnesium alloy AZ80-A study using processing map [J]. *Materials Science and Engineering A*, 2010, 527: 2022–2026.
- [13] LI Miao-quan, LIU Yu-li, WU Shi-chun, WU Xiao-wei. Superplastic deformation of duralumin LY12CZ under an electric field [J]. *Journal of Materials Processing Technology*, 1994, 40(3–4): 385–393.
- [14] AHAMED H, SENTHILKUMAR V. Hot deformation behavior of mechanically alloyed Al6063/0.75Al₂O₃/0.75Y₂O₃ nano-composite-A study using constitutive modeling and processing map [J]. *Materials Science and Engineering A*, 2012, 539: 349–359.
- [15] YANG Yong-biao, ZHANG Zhi-min, ZHANG Xing. Processing map of Al₂O₃ particulate reinforced Al alloy matrix composites [J]. *Materials Science and Engineering A*, 2012, 558: 112–118.
- [16] PRASAD Y V R K. Recent advances in the science of mechanical processing [J]. *Indian Journal of Technology*, 1990, 28(6–8): 435–451.
- [17] RAJAMUTHAMILSELVAN M, RAMANATHAN S, KARTHIKEYAN R. Processing map for hot working of SiC_p/7075 Al composites [J]. *Transactions of Nonferrous Metals Society of China*, 2010, 20(4): 668–674.
- [18] ZHOU Ge, DING Hua, CAO Fu-rong, HAN Yin-ben, ZHANG Bei-jiang. Flow instability criteria in processing map of superalloy GH79 [J]. *Transactions of Nonferrous Metals Society of China*, 2012, 22(7): 1575–1581.

片状粉末冶金 $\text{Al}_2\text{O}_3/\text{Al}$ 复合材料的热变形及加工图

栾佰峰¹, 邱日盛¹, 李春红¹, 杨晓芳¹, 李志强², 张 荻², 刘 庆¹

1. 重庆大学 材料科学与工程学院, 重庆 400044;

2. 上海交通大学 金属基复合材料国家重点实验室, 上海 200240

摘 要: 采用 Gleeble-1500D 热模拟试验机在 300~450 °C、0.001~1.0 s⁻¹ 条件下对不同铝片层厚度的 $\text{Al}_2\text{O}_3/\text{Al}$ 复合材料进行变形行为研究。实验结果表明, 在设定的温度下, 流变应力随着应变速率的增加而增加, 而在设定的应变速率下, 流变应力随着温度的升高而降低。在所采用的实验条件下, 片层 $\text{Al}_2\text{O}_3/\text{Al}$ 复合材料的高温流变行为可以用双曲正弦函数来描述。 $\text{Al}_2\text{O}_3/\text{Al}$ -2 μm 和 $\text{Al}_2\text{O}_3/\text{Al}$ -1 μm 复合材料在进行真应变为 0.6 的热变形时最优加工工艺参数分别为 300~330 °C, 0.007~0.03 s⁻¹ 和 335~360 °C, 0.015~0.06 s⁻¹。而热加工图也明确了此两种复合材料的流变失稳区。

关键词: $\text{Al}_2\text{O}_3/\text{Al}$ 复合材料; 片状粉末冶金; 流变应力; 加工图

(Edited by Yun-bin HE)